Generalization framework for varying characteristics of the firebrand generation and transport from structural fire source

Keisuke Himoto [*], Tatsuya Iwami

National Institute for Land and Infrastructure Management, Tachihara 1, Tsukuba, Ibaraki, 305-0802, Japan

A B S T R A C T

Spot ignition by wind-dispersed firebrands is an important factor in the spread of fire in large outdoor fires. However, the large probabilistic variability in its generation, transport, and ignition processes causes difficulty in quantifying its risk. In this study, a series of wind tunnel experiments was conducted to understand the probabilistically varying characteristics of two among three processes involved in spot ignition, i.e., the generation and transport of firebrands. Analysis samples were generated by combusting a wood crib in an apparatus that simulates the behavior of a fully developed structural fire. The experimental parameters were the ejection height of firebrands, H, crosswind velocity, U_∞, and thickness of wood stick used for assembling the wood crib, d. Utilizing the experimental results, the projected area of a firebrand and its transport distance downwind of a fire source were formulated based on simple physical considerations. However, because the obtained correlations represent deterministic relationships of the parameters, they were further incorporated into probability distributions (a truncated exponential distribution for the projected area and a truncated normal distribution for the transport distance) to enable the consideration of intrinsic variations. The obtained models reasonably reproduced the experimental results for both the projected area and transport distance. Although structural fire is the targeted type of fire source, the proposed models exhibit forms extensible to other types of fire sources.

1. Introduction

Spot ignition due to wind-dispersed firebrands is an important factor in the spread of large outdoor fires, such as urban, wildland, and wildland–urban interface fires. Whereas the effect of radiative and convective heat transfer is limited to areas relatively close to the fire source, wind-dispersed firebrands may cause multiple and discontinuous fire spreads far downwind. Consequently, they can accelerate the enlargement of the burn area significantly.

The behavior of spot ignition due to wind-dispersed firebrands has received significant interest in recent years [1–4]. For analysis purposes, its behavior is often decomposed into three sequential processes: the generation of firebrands from a fire source, transport of firebrands by ambient wind, and ignition of combustibles on landing. Among them, this study focuses on the generation and transport processes. The status of relevant studies can be summarized as follows:

Regarding the generation of firebrands, the behavior has often been analyzed through investigations of actual or prescribed fires [5–12] or through burn experiments on combustibles, including extracted and full-scale samples of vegetation and structures [13–25]. The major aim of those studies is to collect firebrands generated from a fire source and measure their shape and mass. This is because the transport and ignition behaviors of firebrands, which are processes subsequent to the generation process, are dependent on such characteristics of firebrands. However, firebrand characteristics are specific to the generation conditions, which can vary considerably among different fuel types and sizes of the fire source. In terms of hazard analysis, these characteristics must be generalized such that the hazard in an arbitrary situation can be evaluated. Similar attempts have been performed, albeit few. However, they focused more on the thermo–mechanical properties of wooden cylindrical materials and less on the probabilistically varying shape and mass of firebrands intrinsic to the generation process [18,24].

Regarding the transport of firebrands, most early studies solved the equation of motion of a rigid particle in a flow of steady profile for analyzing its behavior [26–36]. In more recent studies, computational fluid dynamics (CFD) simulations have become a dominant approach for tracking the trajectories of firebrands in an unsteady flow field [37–44]. Meanwhile, only a few examples of experimental investigations have been published regarding the transport process owing to the limited availability of experimental facilities [45–48]. Among the existing approaches, CFD simulations can effectively reveal the behavior of

---

Nomenclature

Alphabet

$A_{P(Z)}$	Projected area [cm^2]
B^*	Dimensionless scaling parameter for firebrand transport
d	Thickness of wood stick [cm]
d_P	Representative length of a firebrand [cm]
g	Acceleration due to gravity [m/s^2]
H	Generation height of a firebrand [m]
U_∞	Crosswind velocity [m/s]
V_P	Volume of a firebrand [cm^3]
W_0	Ejection velocity of a firebrand [m/s]
x_P	Transport distance of a firebrand in wind direction [m]

Greek letters

ρ_P	Density of a firebrand [kg/m^3]
ρ_∞	Ambient air density [kg/m^3]

firebrand transport and complements the difficulty of experimental approaches. However, as mentioned above, wind-dispersed firebrands can cause spot ignitions at multiple wide spread locations in a large outdoor fire. For the applied hazard analysis of such behavior [49–56], the high computational cost of CFD simulations becomes an obstacle, particularly because the effect of various uncertain factors must be considered. Meanwhile, analytical approaches are less computationally demanding than CFD simulations. However, they were developed deterministically and the probabilistic variability of the transport process was not considered.

In this study, a generalization framework for the generation and transport of firebrands from a structural fire was proposed; this research focuses on the overall behaviors of firebrands rather than those of an individual firebrand, such that they can be used for the applied hazard analysis of large outdoor fires [49–56]. The models use probabilistic distributions to represent the varying characteristics of the target behaviors. The parameters of the probabilistic distributions were modeled based on simple physical considerations, and their coefficients were statistically determined from the results of a series of wind tunnel experiments.

2. Wind tunnel experiment

In urban fires, which are a threat to Japanese cities, the major source of firebrands that may cause discontinuous fire spread in the downwind region is fire-involved wooden buildings [57]. This is because wooden buildings contain more sources of firebrands (i.e., wooden materials) than non-wooden buildings; however, more importantly, the fall of floors and roof generally occurs in fire-involved wooden buildings in advance of their entire collapse [58]. This creates a strong updraft through the internal space of the building owing to the stack effect and increases the updraft-accompanied force exerted on burning materials inside the building, thereby advancing their detachment from building members.

To analyze the generation and transport behaviors of firebrands from such a structural fire, a series of wind tunnel experiments was conducted. In this study, wood cribs were burnt in an open-top combustion apparatus installed in a boundary layer wind tunnel to simulate the behavior of fire. As thermal degradation progress, the wood cribs lose their structural integrity, and fragments are detached from the main body as they are exposed to the buoyancy-induced updraft formed inside the apparatus. The detached fragments (i.e., firebrands) are ejected out of the apparatus by the updraft and then transported downwind by the crosswind. As the firebrands are under the continuous effect of gravity, they begin descending shortly after ejection and eventually land on the

floor of the wind tunnel. The deposited firebrands were collected using water-filled pans that were strategically placed in the leeward side of the apparatus to measure the shape and mass.

The experiment was conducted using an open-loop boundary-layer wind tunnel, in which the inflow generated by the fan is unaffected by the heat generated from the fire source in the measurement section [59]. The wind tunnel comprises two consecutive measurement sections with different cross-sectional geometries; these sections can be used depending on the nature of the experiment to be conducted. The first measurement section is 10 m long in the wind direction, with an orthogonal cross-section of 5 m × 4 m (width × height). The second measurement section is 15 m long in the wind direction, with an orthogonal cross-section of 5 m × 14 m (width × height). In this experiment, the combustion apparatus and water-filled pans were placed in the second measurement section. In order to avoid any external influences on the experiment due to flow discontinuity, the experimental apparatus was placed at a sufficient distance from the interface of the two measurement sections. Additionally, the inflow velocity profile in front of the experimental apparatus was measured to ensure that it was the desired one [59].

2.1. Experimental apparatus

The combustion apparatus used to generate firebrands with the alignment of 20 water-filled pans in its leeward position is depicted in Fig. 1. The apparatus had a 0.6 m × 0.6 m diffusion burner at its bottom for heating a wood crib placed above it. City gas was used as fuel for the diffusion burner, whose supply rate was measured using an ultrasonic flowmeter. On top of the diffuse burner, a perimeter wall of either 0.8 or 1.2 m high was raised using a 25-mm-thick ceramic board to form a chimney-like compartment. To account for the height of the load cells below the burner, the height of the apparatus H was either 1.08 or 1.48 m. An opening of 0.6 m × 0.4 m (width × height) was made at the bottom of the upwind side of the wall to supply fresh air into the apparatus. A wood crib was placed 0.4 m below the top of the apparatus, regardless of the height of the apparatus, which was exposed to the flame of the diffusion burner at the bottom. The top of the apparatus was left open to imitate a building without floors and roof. This enabled a strong updraft to be created through the internal space of the apparatus owing to the stack effect.

The alignment of the 20 water-filled pans in the downwind region of the combustion apparatus is shown in Fig. 1. It is noteworthy that in Fig. 1, a three-dimensional orthogonal coordinate system is introduced. In the coordinate system, the *X*-axis in the direction parallel to the wind direction, the *Z*-axis in the vertically upward direction, the *Y*-axis in the orthogonal direction to the other axes, and the origin at the center of the downwind side of the combustion apparatus. The size of the water-filled pan was 0.3 m × 0.3 m. The pans were filled with water to immediately quench the firebrands upon landing and to determine the characteristics of the firebrand at that instant. The water-filled pans were placed in the center of evenly spaced meshes (0.6 m × 0.6 m, the same as the cross-sectional geometry of the combustion apparatus) that separated the floor of the measurement section of the wind tunnel. Fourteen of the twenty pans were placed such that their centers were aligned linearly on the *X*-axis. The remaining pans were placed 0.6 and 1.2 m away from the *X*-axis to analyze the dispersion in the direction perpendicular to the wind direction. The collected firebrands were dried in an oven, after which the shape and mass were measured.

2.2. Experimental conditions

The experimental conditions are summarized in Table 1. In this study, six cases (Cases A to F) were investigated under combinations of the following experimental parameters: the height of the firebrand ejection, H (either 1.08 or 1.48 m), crosswind velocity, U_∞ (either approximately 1.5 or 3.0 m/s), and thickness of the wood stick used for
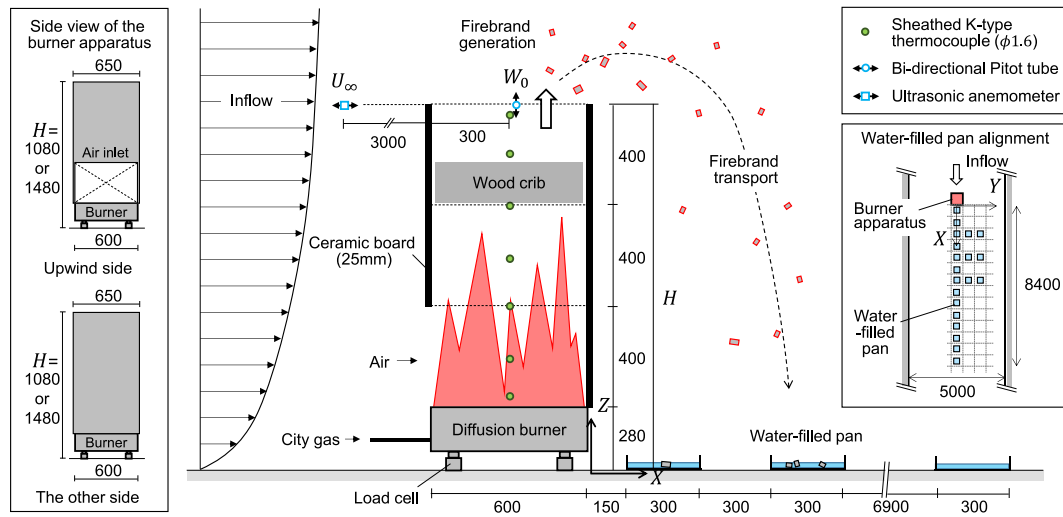
Fig. 1. Combustion apparatus used to generate firebrands ($H = 1.48\,m$) and water-filled pans aligned downwind of the apparatus.

Table 1
Experimental condition for firebrand generation and transport. Experimental parameters were ejection height, H, crosswind velocity, U_∞, and thickness of wood stick, d.

Case	Ejection height H (m)	Crosswind velocity U_∞ (m/s)	Thickness of wood stick d (mm)	Initial mass of wood crib (kg)	Mean total heat release rate (kW)	Number of collected firebrands
A1	1.08	1.41	105	14.63	336.16	102
A2		1.45		16.29	336.47	131
A3		1.48		16.29	321.99	172
A4		1.53		16.17	335.40	205
A5		1.43		16.93	320.66	168
B1	1.08	3.06	105	15.63	330.60	155
B2		3.05		14.86	286.02	168
B3		3.09		15.56	317.40	187
B4		3.10		15.69	341.10	185
B5		3.01		15.93	333.27	207
C1	1.48	1.53	50	10.07	490.08	17
C2		1.55		10.05	489.45	33
C3		1.64		10.20	493.86	53
C4		1.47		9.96	486.70	12
C5		1.63		10.23	494.63	28
D1	1.48	2.98	50	10.73	509.65	37
D2		3.22		10.39	499.44	56
D3		2.96		10.12	491.41	53
D4		2.94		10.11	491.10	36
D5		2.98		9.97	487.16	37
D6		2.84		21.09	702.95	116
E1	1.48	1.47	105	15.77	347.42	81
E2		1.47		14.42	334.09	69
E3		1.45		15.24	331.80	95
E4		1.49		15.98	329.13	68
E5		1.46		17.60	343.06	129
F1	1.48	3.04	105	14.88	338.63	104
F2		3.05		15.37	343.47	109
F3		3.08		15.16	341.40	108
F4		3.08		16.00	344.05	152
F5		3.01		14.99	345.41	113

assembling wood cribs, d (either 50 or 105 mm). However, each case was repeated at least five times to ensure the number of samples for the statistical analysis. Among the six tested cases, the cases in group D tended to have a small sample size. Hence, an additional test was conducted for Case D to increase the sample size with double the number of wood cribs by stacking one on top of the other (Case D6). The total numbers of firebrand samples collected were 778, 902, 143, 335, 442,

and 586 for Cases A to F, respectively.

The crosswind velocity, U_∞, was adjusted by controlling the rotation rate of the fan in two steps. U_∞ was measured using an ultrasonic anemometer located 3 m upstream of the combustion apparatus at a height of 1.48 m. The average U_∞ was 1.50 m/s for the lower cases (Cases A, C and E) and 3.03 m/s for the higher cases (Cases B, D and F). Details of the flow field characteristics in the boundary layer wind tunnel are described in Ref. [59].

As a source of firebrands, sticks of Japanese cedar were used to assemble a wood crib. The sizes of the wood sticks used were 50 mm × 50 mm × 550 mm ($d = 50$ mm) for the small cross-section cases (Cases C and D) and 105 mm × 105 mm × 550 mm ($d = 105$ mm) for the large cross-section cases (Cases A, B, E, and F). The configuration of each wood crib is summarized in Table 2. The assembled wood cribs were dried in an oven at 105 °C for at least 3 days and wrapped in film wraps until immediately before the experiment to prevent an increase in the moisture content. The average mass of the wood cribs at the beginning of the experiment were 10.18 and 15.67 kg for $d = 50$ mm (except for Case D6) and $d = 105$ mm, respectively. Temporal changes in the mass of the wood cribs in the combustion apparatus were measured using four load cells installed at the bottom of the apparatus. Fig. 2 shows the ensemble averages of the mass loss rates measured at least five times for each case. It shows that for the same d, the change in the mass loss rate over time was almost identical and the least affected by the height of the combustion apparatus, H, or the flow velocity, U_∞. For all d, the mass loss rate reached its maximum at approximately 1.5 min after ignition and then started to decrease gradually. The duration of wood crib combustion was approximately 10 and 30 min for $d = 50$ and 105 mm, respectively.

For an assumed combustion heat of wood cribs of 16.09 MJ/kg [61], the average rate of heat release was 141.21 kW for $d = 50$ mm (except for Case D6) and 301.68 kW for $d = 105$ mm. By including the rate of

Table 2
Configuration of the wood cribs used as a source of firebrands.

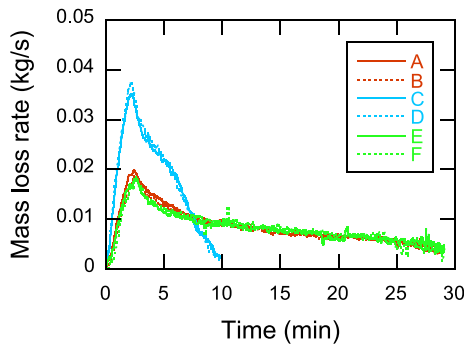| Type	Small cross-section	Large cross-section
Thickness of wood stick d (mm)	50	105
Length of wood stick (mm)	550	550
Number of layers	4	2
Number of sticks per layer	6	3
Porosity (Volumetric)	0.455	0.427
Porosity factor [60]	0.0054 (0.0028 for Case D6)	0.00191

Fig. 2. Ensemble averages of mass loss rate of wood cribs after ignition.

heat release for the city gas combustion (fixed at 191.7 kW for all cases), the rates of total heat release in the combustion apparatus were 332.88 and 593.35 kW for $d = 50$ and 105 mm, respectively.

In the combustion apparatus, sheathed K-type thermocouples ($\varphi 1.6$ mm) were set at five locations (Cases A and B) or seven locations (Cases C, D, E, and F) for the temperature measurement (cf. Fig. 1 for thermocouple locations). Fig. 3 shows the average temperature inside the apparatus during combustion. The highest temperatures were recorded in Cases C and D, in which wood cribs with small cross-sections ($d = 50$ mm) were used. In general, the internal temperatures were higher with lower H, lower U_∞, and smaller d.

A bi-directional Pitot tube was set in the center of the outlet at the top of the combustion apparatus to measure the ejection velocity, W_0. Fig. 4 shows the average W_0 during the test, with error bars indicating the standard deviations. The average W_0 ranged from $2.46 m/s$ (Case B) to $4.10 m/s$ (Case E). The effects of the experimental parameters (H, U_∞, and d) were not as apparent as in the case of the internal temperature, as shown in Fig. 3. However, the order of magnitude of W_0 corresponded primarily to that of the temperature measured at the thermocouple nearest to the top. In other words, the higher the outlet temperature, the larger was the ejection velocity, W_0.

3. Generation

The measurement results of the collected firebrands are summarized in Table 3. In this section, the shape and mass of the firebrands, including their probabilistic variabilities, were generalized using the experimental results for the analysis of the subsequent processes of the spot ignitions by wind-dispersed firebrands.

3.1. Shape

For the shape, the images of each firebrand placed on a horizontal plane in a stable state were captured individually using three charge-coupled device (CCD) cameras simultaneously from each axis of the three-dimensional orthogonal coordinate system (*xyz*-axes) centered on the firebrand (Fig. 5). Unless the difference was not discernible, the orientation of the firebrand was adjusted such that the directions of the
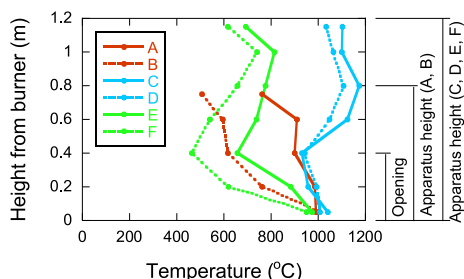

Fig. 3. Average temperature distributions inside combustion apparatus.
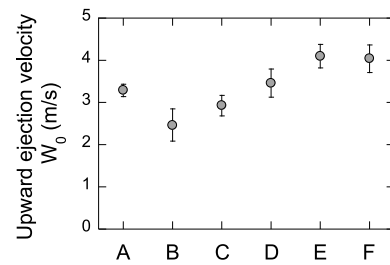

Fig. 4. Average ejection velocities at top of combustion apparatus. Error bars indicate standard deviations.

longer and shorter sides were parallel to the *x*- and *y*-axes, respectively. The projected area and the three side lengths of the collected firebrands were measured using image analysis software (Adobe Photoshop). To convert the scale of the firebrand in an image to the real scale, an aluminum cube ($1\ cm \times 1\ cm \times 1\ cm$) was placed next to a firebrand as a reference, and images were captured such that they were within the same angle of view.

(1) Projected area (z)

Among the images captured from the three orthogonal directions, the image captured from the direction parallel to the *z*-axis was used to measure the projected area of the firebrand, $A_{P(Z)}$. As shown in Table 3, the average $A_{P(Z)}$ of the firebrand collected in the present experiment was in the order of $\sim 10^{-1}$ cm^2, whereas those of previous full-scale experiments were in the order of $\sim 10^0 - 10^1$ cm^2 [21,25]. The smaller $A_{P(Z)}$ in the present experiment is likely due to the relatively low heat release rate of the fire source and the velocity of the cross-wind, both of which affect the forces acting on the firebrands.

As shown in Table 3, the medians of $A_{P(Z)}$ descended in the order of Cases D, E, F, C, A, and B. This indicates that the $A_{P(Z)}$ of the firebrands tended to be smaller if they were ejected from the lower position, H (Cases A and B). Possible causes of the difference in $A_{P(Z)}$ in association with the difference in H are the fire size inside the apparatus and the ejection velocity from the apparatus, W_0; however, the crosswind velocity, U_∞, thickness of wood stick, d, and internal temperature of the combustion apparatus (Fig. 3) were not considered as they were not indicative of the order of $A_{P(Z)}$. Among the two possible causes, the effect of H on the mass loss rate of the wood cribs (cf. Cases E and F in Fig. 2) was negligible, i.e., the effect of mass loss rate due to wood crib combustion on $A_{P(Z)}$ can be omitted. As for the other possible causes, the medians of $A_{P(Z)}$ were plotted vs. W_0, as shown in Fig. 6. Although the range of W_0 was limited in this experiment the two parameters were correlated, i.e., $A_{P(Z)}$ increased with W_0. Hence, upon ejection, the updraft-induced drag force exerted on the firebrand is considered to be of the same order as the gravity, i.e.,

$$A_{P(Z)}\rho_\infty W_0^2 \sim \rho_P V_P g, \tag{1}$$

where ρ_∞ is the ambient air density, ρ_P is the firebrand density, V_P is the firebrand volume, and g is the acceleration due to gravity. In Eq. (1), the force receiving area is assumed to be equivalent to $A_{P(Z)}$. Based on d_P as the representative length of the firebrand, the projected area and volumes are of the order $A_{P(Z)} \sim d_P^2, V_P \sim d_P^3$; thus, $V_P \sim A_{P(Z)}^{3/2}$. Hence, Eq. (1) can be transformed to

$$A_{P(Z)} \sim \left(\frac{\rho_\infty}{\rho_P}\frac{W_0^2}{gH}\right)^2 H^2 \tag{2}$$

In this equation, $A_{P(Z)}$ is scaled to the fourth power of W_0.

The relative frequency distribution of $A_{P(Z)}$ for each case is shown in Fig. 7. All the distributions were similar in that they have a high

K. Himoto and T. Iwami

Fire Safety Journal 125 (2021) 103418

Table 3
Shape and mass of collected firebrands. Values, highlighted values, and values in parentheses are the averages, medians, and standard deviations, respectively.

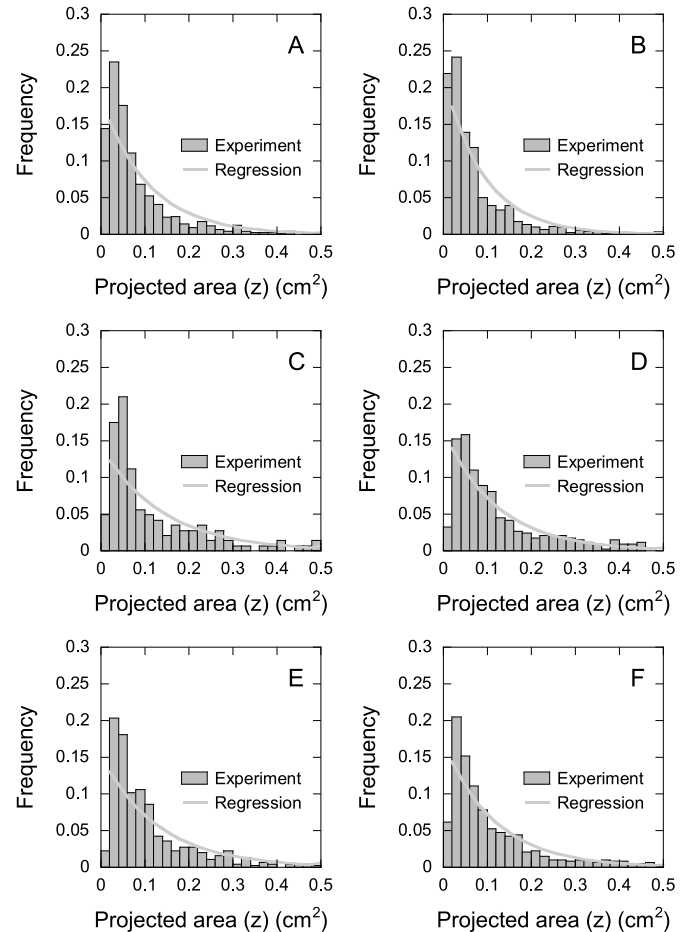| Case	Number of collected firebrands	Projected area (z) $A_{P(Z)}$ (cm^2)	Side length (x) (cm)	Side length (y) (cm)	Side length (z) (cm)	Surface area A (cm^2)	Volume V_P (cm^3)	Density ρ_P (kg/m^3)
A	778	0.102 / 0.0529 / (0.177)	0.448 / 0.359 / (0.303)	0.261 / 0.216 / (0.176)	0.179 / 0.150 / (0.114)	0.360 / 0.178 / (0.644)	0.0282 / 0.00593 / (0.120)	60.6 / (12.9)
B	902	0.0884 / 0.0448 / (0.158)	0.404 / 0.328 / (0.284)	0.240 / 0.202 / (0.165)	0.164 / 0.135 / (0.114)	0.308 / 0.150 / (0.551)	0.0225 / 0.00456 / (0.0831)	64.3 / (7.74)
C	143	0.143 / 0.0699 / (0.194)	0.472 / 0.398 / (0.277)	0.397 / 0.294 / (0.245)	0.252 / 0.192 / (0.185)	0.582 / 0.264 / (0.839)	0.0585 / 0.0107 / (0.157)	29.7 / (13.4)
D	335	0.178 / 0.0902 / (0.350)	0.560 / 0.463 / (0.358)	0.375 / 0.306 / (0.276)	0.238 / 0.194 / (0.165)	0.649 / 0.317 / (1.30)	0.0733 / 0.0141 / (0.345)	51.3 / (20.6)
E	442	0.120 / 0.0780 / (0.132)	0.506 / 0.434 / (0.272)	0.307 / 0.267 / (0.157)	0.191 / 0.167 / (0.104)	0.414 / 0.263 / (0.484)	0.0280 / 0.0104 / (0.0647)	63.6 / (10.5)
F	586	0.145 / 0.0729 / (0.241)	0.528 / 0.433 / (0.333)	0.317 / 0.268 / (0.199)	0.204 / 0.167 / (0.129)	0.495 / 0.258 / (0.786)	0.0426 / 0.0102 / (0.151)	74.5 / (17.5)
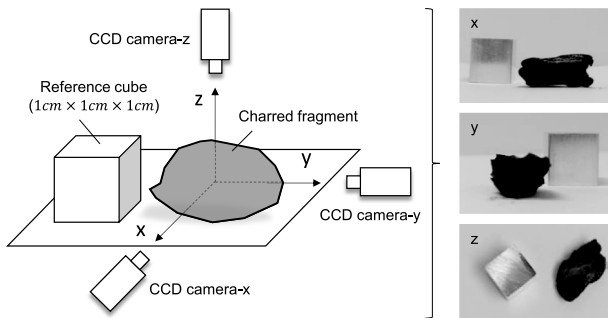
Fig. 5. Images of firebrand captured from three orthogonal directions simultaneously with a reference cube in the same angle of view.
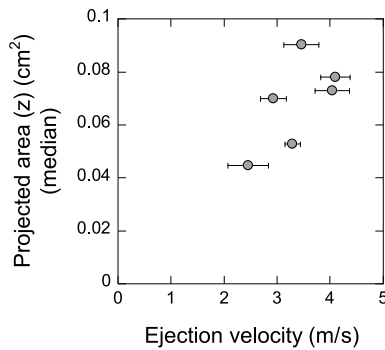
Fig. 6. Relationship between ejection velocity at outlet of combustion apparatus and projected areas of firebrands (median). Error bars are the standard deviations.

Fig. 7. Relative frequency distribution of projected area of firebrands overlaid by estimated exponential distribution.

proportion of relatively small firebrands (i.e., small $A_{P(Z)}$) with a long tail toward large firebrands. Such a large variability in size could result in a large probabilistic variability in the transport and ignition behaviors. However, Eq. (2) provides a deterministic relationship for $A_{P(Z)}$ and does not express the probabilistic variability. Hence, the distribution of

$A_{P(Z)}$ was approximated by a known probability distribution, and its parameters were modeled using the correlation shown in Eq. (2). Considering the unimodal profile of the measured distribution, the log-normal distribution was used to test its applicability. However, the result was unsatisfactory; although the peak of the log-normal distribution shifted with the average and standard deviation of the firebrand size, the peak of the actual distribution was insensitive to the experimental parameters (i.e., the peaks were below $0.06 cm^2$ for all the tested cases). It was suggested that the unimodal profile of the measured distributions was not attributed to its intrinsic nature but to the experimental limitation that minute firebrands were not collectable. Hence, the exponential distribution, a monotonically decreasing function with a peak at zero, was selected for regressing the measured distribution. Considering the experimentally collectable range of the firebrands, the truncated form of the exponential distribution was adopted, i.e.,

$$q(x|\beta) = p(x|\beta, x \geq L) = \frac{p(x)}{\int_L^\infty p(x) dx}, \tag{3}$$

In Eq. (3), β is the rate parameter, and L is the lower bound of the random variables, which was set to 0.01. Upon modeling β using the correlation in Eq. (2), it should be noted that the exponential distribution exhibited a longer tail (a larger proportion of firebrands with large $A_{P(Z)}$) with smaller values of β. Hence, β must be a monotonically decreasing function of the right-hand side of Eq. (2). In addition, β must be a positive real number and that the firebrand is not expected to be generated when the right-hand side of Eq. (2) is zero (i.e., $W_0 = 0$). To satisfy these requirements, the following formulation was assumed:

$$A_{P(Z),i} \sim q(\beta_i) \tag{4}$$

$$\beta_i = \left[a + b \left(\frac{\rho_\infty}{\rho_P} \frac{W_{0,i}^2}{g H_i} \right)^2 H_i^2 \right]^{-1}, \tag{5}$$

where a and b are the parameters to be estimated.

In this study, the Bayesian approach, which employs a Markov chain Monte Carlo (MCMC) simulation to obtain samples from the target posterior distribution of the parameters, was used to estimate the model [62].

$$p(\theta|Y) = \frac{p(Y|\theta) p(\theta)}{p(Y)} \propto p(Y|\theta) p(\theta), \tag{6}$$

where $p(\theta|Y)$ is the posterior distribution, $p(Y|\theta)$ is the likelihood, $p(\theta)$ is the prior distribution, $p(Y)$ is the normalization constant, θ is the model parameter, and Y is the base data. Four independent sequences of Markov chains were created with starting points obtained from a non-informative distribution that can be guaranteed to play a minimal role in the posterior distribution. The number of iterations for each sequence was 5000, the first half of which was discarded to diminish the effect of the starting values. Table 4 shows the results of the parameter estimation. The convergence of the Markov chains was monitored based on the following metric, which compares the between-sequence variance B and the within-sequence variance W [62]:

$$\hat{R} = \sqrt{\frac{(m-1)W + B}{mW}}, \tag{7}$$

Table 4
Result of parameter estimation for projected area. Estimates are maximum a posteriori estimates of posterior distributions. S.D. is the standard deviation; 2.5 % and 97.5 % are the top and bottom bounds of the credible interval, respectively.

Parameter	Estimate	S.D.	2.5 %.	97.5 %.	$\hat{R}$
a	0.0865	0.00359	0.0796	0.0936	1.00
b	42.4	5.94	30.9	54.0	1.00

where m is the number of iterations. The upper bound threshold for convergence, i.e., $\hat{R} < 1.1$, was required for all the quantities of interest. In addition, the χ^2-test of goodness-of-fit at a significance level of 5% was performed to evaluate the agreement between the theoretical model and the measurement data. For all the cases, the results demonstrated that the theoretical models were not statistically insignificant. The obtained truncated exponential distributions were overlaid on the measured distributions shown in Fig. 7. Although there were discrepancies between the theoretical model and the measurement data, especially in the small $A_{P(Z)}$ range, the overall agreement was reasonable, demonstrating the validity of the model formulation shown in Eqs. (4) and (5).

(2) Volume

The projected area, $A_{P(Z)}$, is the planar geometry of the firebrand viewed from one direction. To describe the three-dimensional geometry of the firebrands, the length ratios of the y- and z-axes to the x-axis were obtained, as shown in Fig. 8. The result differed from that of Case C with a small number of samples. However, the range of the average range of the length ratios was 0.60–0.70 for y/x and 0.38–0.43 for z/x for the other cases. This implies that the shape of the collected firebrands was more granular or flaky than rod-like or platy in this experiment. Hence, the surface area, A, and volume, V_P, were estimated by approximating the shape with an ellipsoid using the following equations:

$$A \cong 4\pi \left(\frac{a^P b^P + b^P c^P + c^P a^P}{3} \right)^{1/P} \tag{8}$$

$$V_P = \frac{4}{3} \pi abc, \tag{9}$$

where a, b, and c are the lengths in the x-, y-, and z-axes, respectively. $P(=1.6075)$ is a constant. The estimated A and V_P for each case are listed in Table 3. The distributions of $A_{P(Z)}$ and V_P are compared in the percentile plots shown in Fig. 9. Similar results were obtained for each case between $A_{P(Z)}$ and V_P. However, reflecting the scale relationship, $A_{P(Z)} \sim d_P^2$ and $V_P \sim d_P^3$, the tails of the distributions were shorter for $A_{P(Z)}$ than for V_P. Among the six tested cases, the tails of the distributions were relatively long in Cases C and D (smaller thickness of wood stick, d), i.e., the proportion of large firebrands was relatively large. As estimated using Eq. (2) ($A_{P(Z)} \propto \rho_P^{-2}$), this is attributable to the relatively small density of the firebrands, ρ_P, as will be discussed in the subsequent section.

3.2. Density and mass

The collected firebrands were dried in an oven, and their weights were measured on an electronic scale that had a measurement accuracy of 1/100 g. However, because the individual weights of some of the
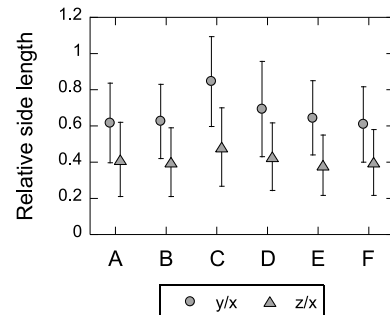
Fig. 8. Medians of length ratios of y- and z-axes to x-axis of collected firebrands. Error bars indicate standard deviations.
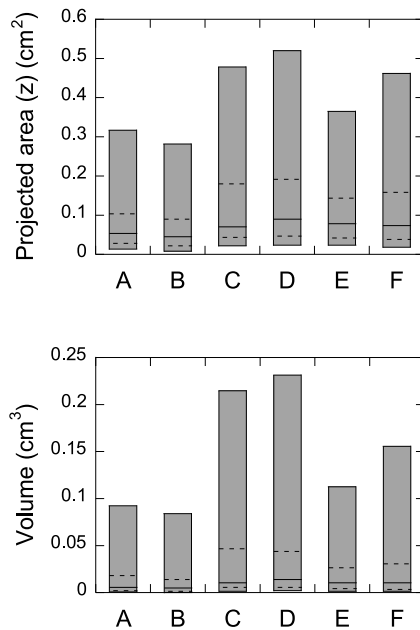
Fig. 9. Percentile plots of measured projected area and estimated volume of collected firebrands. Solid lines inside boxes are the medians; dotted lines are the 25th and 75th percentiles; bottom and top bounds of the boxes are the 5th and 95th percentiles, respectively.

firebrands were out of the range of the electronic scale, the total weight was measured for each test case and converted to the density, ρ_P, by dividing it by the sum of the estimated volumes. Therefore, the distributions were not available, similarly for $A_{P(Z)}$ and V_P. As shown in Table 3, the mass of the firebrand collected in the present experiment was in the order of $\sim 10^{-4}$ g. Although a full-scale experiment with an order of $\sim 10^{-3} - 10^{-1}$ g has been reported [14], experiments with a larger order, i.e., $\sim 10^{-2} - 10^{0}$ g, have also been noted [21,25]. Overall, the firebrands collected in this experiment were smaller than those collected in full-scale experiments.

Fig. 10 shows the average ρ_P for each case with the error bars indicating the standard deviations; the overall average was 59.4 kg/m³. Previous studies regarding the burn experiment of a three-story wooden building reported that ρ_P ranged from 76 to 86 kg/m³ [21], which was similar to the experimental results of this study. Among the six tested cases, ρ_P for Cases C and D (smaller thickness of wood stick, d) were smaller than those for the other cases. This is attributable to the difference in the internal temperature of the combustion apparatus, as shown in Fig. 3. The wood cribs were exposed to intense heating in Cases C and D compared with the other cases.

The amount of firebrands generated relative to the initial weight of the wood crib is important for assessing the applied hazard analysis of wind-dispersed firebrands as it is generally unknown and must be estimated from the conditions of the fire source. In this experiment, not all
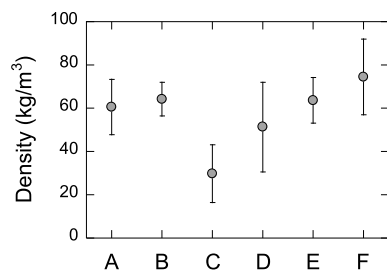
of the generated firebrands were collected as they dispersed widely, whereas the number of water-filled pans used for collection was limited. For estimating the firebrand weight in each 0.6 m × 0.6 m mesh downwind of the combustion apparatus, the estimated number of firebrands deposited in each mesh was multiplied by the average weight of the firebrand. For the meshes with water-filled pans, the number of firebrands in each mesh was estimated by multiplying the collected number of firebrands per unit area by the mesh area. For the meshes without a water-filled pan, the number of firebrands was estimated by linearly interpolating or extrapolating the number of nearby meshes. Fig. 11 shows the proportion of the total mass of generated firebrands to the initial mass of the wood crib. The proportion ranged from 0.00526 % (Case E) to 0.0176 % (Case D). In a previous study where wood cribs were similarly burned as the firebrand source, it was reported that the proportion ranged from 0.06 % to 1.64 % [16]. In another study where Korean pine trees and Douglas-fir trees were burned, it was reported that the proportion ranged from 0.08 % to 0.28% [15]. The proportion in this study was smaller because the combustibles were not burned in an open environment; instead, they were burned within an enclosed apparatus. Hence, only firebrands ejected from the combustion apparatus were collected. In other words, a considerable amount of burning fragments (i.e., potential firebrands) were assumed to have burnt out inside the combustion apparatus as their ejection was blocked by the perimeter wall. This result implies that the weight proportion in urban fires (buildings are the major combustibles) is expected to be smaller than that in forest fires (vegetation is the major combustible).

4. Transport

The measured deposition distributions of the firebrands in the wind and orthogonal directions are summarized in Table 5. In this section, the distributions of the firebrand deposition, including the probabilistic variability, are generalized using the experimental results to determine the possible ignition locations in the downwind region of a fire source.

4.1. Deposition distribution

Fig. 12 shows the relative frequency distributions of the firebrand deposition in the wind direction ($Y = 0$ m, along the X-axis). The distributions can be viewed as unimodal with asymmetrical tails to the peak in all cases. The descending order of the average transport distances, x_P, was Cases D, F, B, C, E, and A. In general, the average x_P was larger with a higher ejection height, H, (Cases C, D, E, and F), larger crosswind velocity U_∞ (Cases B, D, and F), and smaller thickness of wood stick, d, (Cases C, and D). The relative frequency distribution shows the breakdown of the projected area, $A_{P(Z)}$, categorized into three group sizes ($-0.05 cm^2$, $0.05 - 0.1\ cm^2$, $0.1 cm^2 -$). This indicates that the ratio of firebrands with small $A_{P(Z)}$ increased as the deposition location became farther from the fire source.

Fig. 13 shows the relative frequency distribution of firebrands collected in water-filled pans placed in the direction parallel to the Y-axis ($X = 1.5, 2.7$, and 3.9 m). In contrast to the result in the wind

Fig. 10. Average firebrand density with error bars indicating standard deviations.
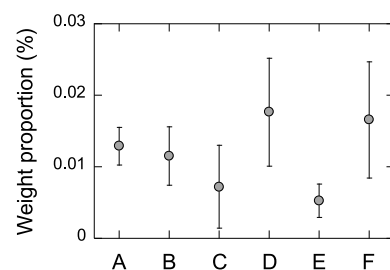

Fig. 11. Proportion of total mass of generated firebrands to initial wood crib mass. Error bars indicate standard deviations.

Table 5

Deposition distribution of firebrands. Values, highlighted values, and values in parentheses are the averages, medians, and standard deviations, respectively.

Case	Wind direction (X)		Orthogonal direction (Y)		
	Number of firebrands	x_P (m)	X (m)	Number of firebrands	Variation
A	656	2.03 1.5 (1.35)	1.5	209	(0.323)
			2.7	93	(0.335)
			3.9	42	(0.398)
B	695	3.42 3.3 (1.82)	1.5	90	(0.336)
			2.7	142	(0.311)
			3.9	86	(0.283)
C	116	3.39 2.7 (1.76)	1.5	22	(0.376)
			2.7	25	(0.415)
			3.9	23	(0.409)
D	272	4.44 4.5 (1.91)	1.5	13	(0.275)
			2.7	40	(0.290)
			3.9	68	(0.309)
E	374	2.06 1.5 (1.31)	1.5	131	(0.300)
			2.7	60	(0.298)
			3.9	27	(0.360)
F	477	3.46 3.3 (1.78)	1.5	67	(0.297)
			2.7	95	(0.326)
			3.9	94	(0.292)

direction ($Y = 0$ m, along the X-axis), the effect of the experimental parameters (H, U_∞, and d) on the distribution was not apparent. It is noteworthy that in each figure that compose Fig. 13, the sum of the bin values is below 1, although a value of 1 was assumed for a relative frequency distribution. This is because the water-filled pans for collecting the firebrands were placed only on one side of the area to the X-axis ($Y \geq 0$). Hence, the deposition distribution on the other side of the area to the X-axis ($Y < 0$) was estimated by mirroring the deposition distribution in $Y \geq 0$. The standard deviations of the deposition distribution in the Y-axis direction shown in Table 3 were also obtained in this manner.

4.2. Model development

To analyze the dispersal distribution of the firebrands, a model for the transport distance, x_P, was derived based on simple physical considerations. Fig. 14 shows a schematic of the model, in which the motion of a firebrand ejected vertically upward from the top of a fire source at H is depicted. Regarding the motion in the Z-axis direction, the firebrand ejected from the fire source increases the altitude owing to the updraft-attributed inertia. However, because the firebrand is continuously subjected to gravity, it begins descending after a time period and eventually settle on the ground. Regarding the motion in the X-axis direction, the firebrand is transported downwind by the crosswind. The distance by which the firebrand is transported in the downwind direction before it eventually settled on the ground is the transport distance, x_P.

The assumptions introduced to model the transport distance of a firebrand, x_P, are as follows:

- The firebrand is assumed to exit from the influential range of the buoyant plume above the fire source shortly after ejection. Thus, in the Z-axis direction, the effect of the updraft above the fire source is represented by the initial ejection velocity, and the only force acting on the firebrand during dispersion is gravity. In the X-axis direction, the firebrand settles under the dominant effect of ambient wind.
- The ambient gas density, ρ_∞, is negligible compared to the firebrand density, ρ_P.

- The time required for the firebrand to settle on the ground after ejection is short; hence, the effect of changes in the density, ρ_P; projected area, A_P; and volume, V_P with respect to time can be neglected.
- The drag force acting on the firebrand during dispersion can be scaled by the initial drag force when ejected from the fire source, i.e., $\propto A_P \cdot \frac{1}{2}\rho_\infty U_\infty^2$, regardless of its relative velocity to the ambient wind.

The first assumption is adequate, particularly under strong wind conditions, during which the dispersion of firebrands is the most important aspect. However, the third and fourth assumptions are relatively weak assumptions that may not be adequate for firebrands with long dispersion times.

Regarding the motion in the Z-axis direction, the equation of motion of a firebrand partible can be expressed as follows:

$$\rho_P V_P \frac{dw_P}{dt} \sim -\rho_P V_P g, \tag{10}$$

where ρ_P is the firebrand density, V_P is the firebrand volume, w_P is the firebrand velocity in the Z-axis direction, t is the time, and g is the acceleration due to gravity. If the firebrand is ejected from a height H with an initial velocity of $w_P = W_0$, then Eq. (10) can be transformed into

$$W_0 t - \frac{1}{2} g t^2 \sim -H \tag{11}$$

This can be solved to yield the time for the firebrand to settle on the ground, t_P, as follows:

$$t_P \sim \frac{W_0}{g} \left(1 + \sqrt{1 + \frac{2gH}{W_0^2}}\right) \tag{12}$$

Regarding the motion in the X-axis direction, the drag force due to the crosswind is assumed to be the dominant force exerted on the firebrand. Therefore,

$$\rho_P V_P \frac{du_P}{dt} \propto A_P \cdot \frac{1}{2}\rho_\infty U_\infty^2, \tag{13}$$

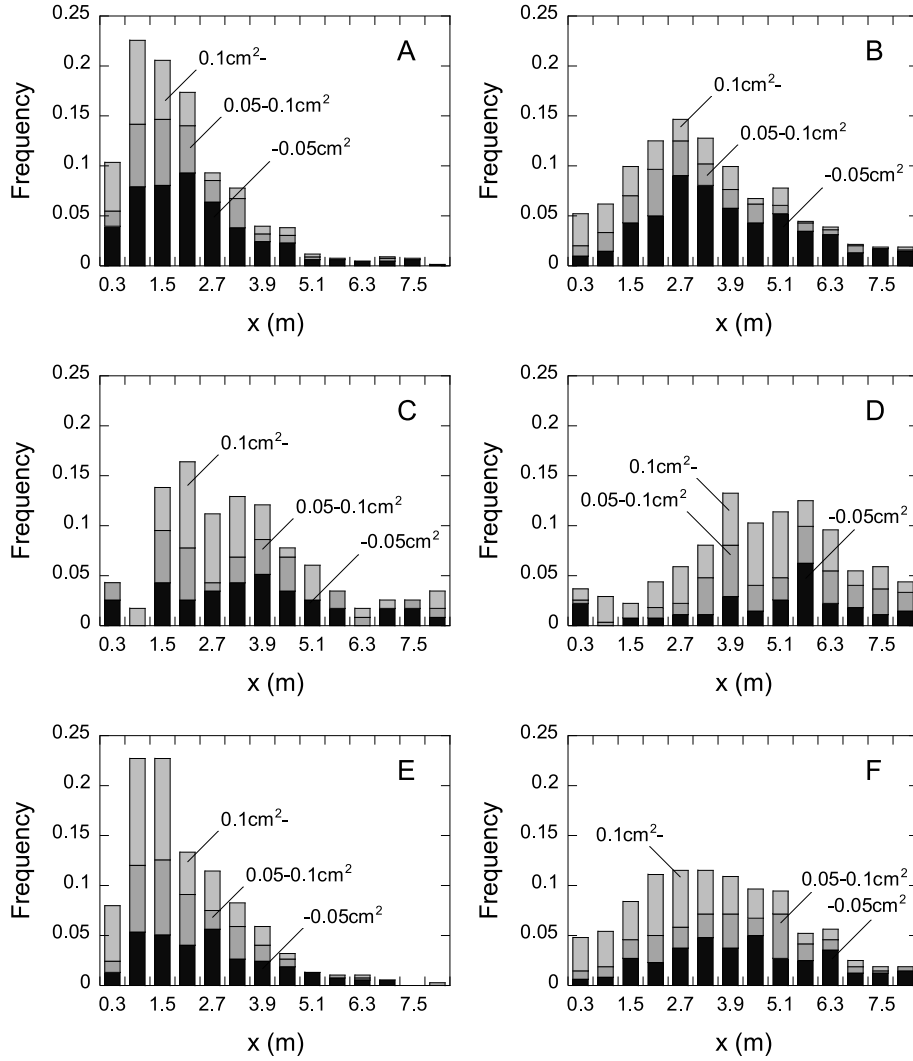where A_P is the area of the firebrand projected onto the plane orthogonal

Fig. 12. Relative frequency distribution of firebrand deposition in wind direction ($Y = 0$ m, along X-axis).

to the wind direction, and U_∞ is the crosswind velocity. By integrating Eq. (13) twice with respect to time, t, the position of the firebrand, x_P, can be obtained as follows:

$$x_P \propto \left(\frac{A_P}{V_P}\right)\left(\frac{\rho_\infty}{\rho_P}\right)U_\infty^2 \cdot t^2 \tag{14}$$

This equation can be further transformed by substituting t_P into Eq. (12) as follows:

$$x_P \propto \left(\frac{U_\infty W_0}{g\sqrt{d_P H}}\right)^2 \left(\frac{\rho_\infty}{\rho_P}\right)\left(1 + \sqrt{1 + \frac{2gH}{W_0^2}}\right)^2 \cdot H \equiv B^* \cdot H \tag{15}$$

where B^* is the dimensionless scaling parameter. In transforming the equation, the term, V_P/A_P, is substituted with the representative length of the firebrand, d_P. It is noteworthy that this expression is applicable to an arbitrary type of fire other than a structural fire because the assumptions introduced in the derivation process are of the general transport behavior, i.e., not specific to a structural fire.

4.3. Model validation

Fig. 15 shows the analysis results of the experimental data using Eq. (15), in which the data points represent those of individual firebrands. The measured x_P is on the vertical axis, and the right-hand side of Eq. (15) is represented on the horizontal axis. The data points indicated a substantial variation. However, the relative frequency distributions of the data points indicated a monotonic shift in the peaks, thereby supporting the adequacy of Eq. (15) for correlating the experimental data. As U_∞, W_0, ρ_P, and H, involved in the parameter on the horizontal axis, $B^* \cdot H$, can be considered as constants in each figure, the only variable that affects the value of $B^* \cdot H$ is the firebrand density, d_P. In other words, the data points on the right are the ones with smaller d_P. Note that, in all cases, the values of the bins between $x_P = 4$ and 5 m were smaller than those of the other ranges. Although the reason for this is not yet clear, it might be possible that the installation of the combustion apparatus in the boundary layer wind tunnel caused a disturbance in the flow field, thereby impeding the accumulation of firebrands locally.

Similar to the case of the projected area of the firebrand, $A_{P(Z)}$, Eq. (15) provides a deterministic relationship for x_P but does not express the probabilistic variability. Hence, the distribution of x_P was approximated by a known probability distribution and its parameters were modeled using the correlation shown in Eq. (15). The parameters of x_P including their probabilistic variation were statistically estimated using the Bayesian approach, which is the same procedure used to estimate $A_{P(Z)}$ in Section 3.1. In the estimation, a log-normal distribution was first tested as the probability distribution. However, the result was unsatisfactory because the relative frequency distributions of x_P (Fig. 15) were not as skewed nor as wide as the log-normal distribution. As an alternative, the applicability of the normal distribution was tested. However,
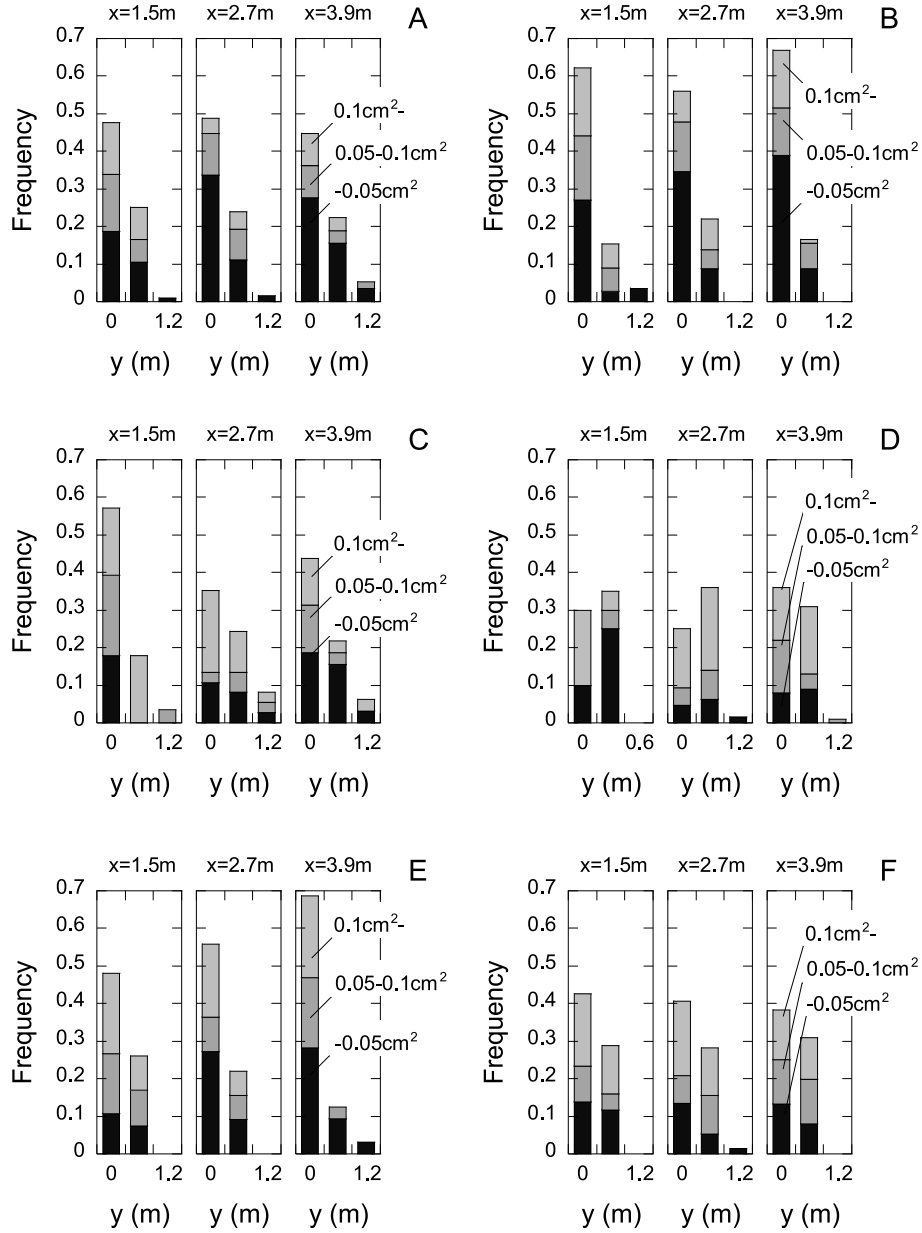
Fig. 13. Relative frequency distribution of firebrands deposition in direction parallel to Y-axis (X = 1.5, 2.7, and 3.9 m).
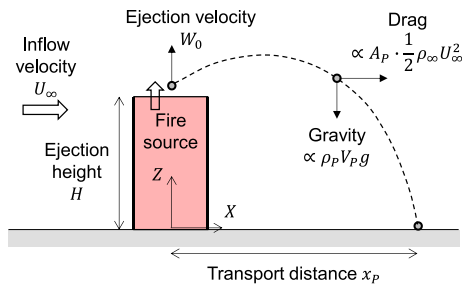

Fig. 14. Transport distance of a firebrand ejected from the top of a fire source in the crosswind region.

the normal distribution is unfavorable in this context as the random variable can have a negative value. In other words, if used without modification, it yields an unrealistic estimate, i.e., the firebrands may disperse in the upwind direction. Hence, the following truncated normal

distribution that bounds the range of the random variables was used:

$$q(x|\mu, \sigma) = p(x|\mu, \sigma, x \geq 0) = \frac{p(x)}{\int_0^\infty p(x)dx} = \frac{p(x)}{1 - \Phi(-\mu/\sigma)} \quad (16)$$

$$p(x|\mu, \sigma) = \frac{1}{\sqrt{2\pi}\sigma} \exp\left\{-\frac{(x-\mu)^2}{2\sigma^2}\right\},$$

where μ is the average, σ is the standard deviation, and Φ is the cumulative distribution function of the standard normal distribution. It is noteworthy that in the present experiment, the water-filled pans were placed up to 8.1 m downwind of the fire source, as indicated by the red dotted lines in Fig. 15. Therefore, the firebrands that would have been dispersed beyond this range were not collected. This signifies that the upper bound of the measured data was truncated. Thus, the truncation of measured data was considered when performing the statistical estimation:

$$x_{P,i} \sim q(\mu_i, \sigma_i) \text{ with } x_{P,i} \leq x_{UB} \quad (17)$$
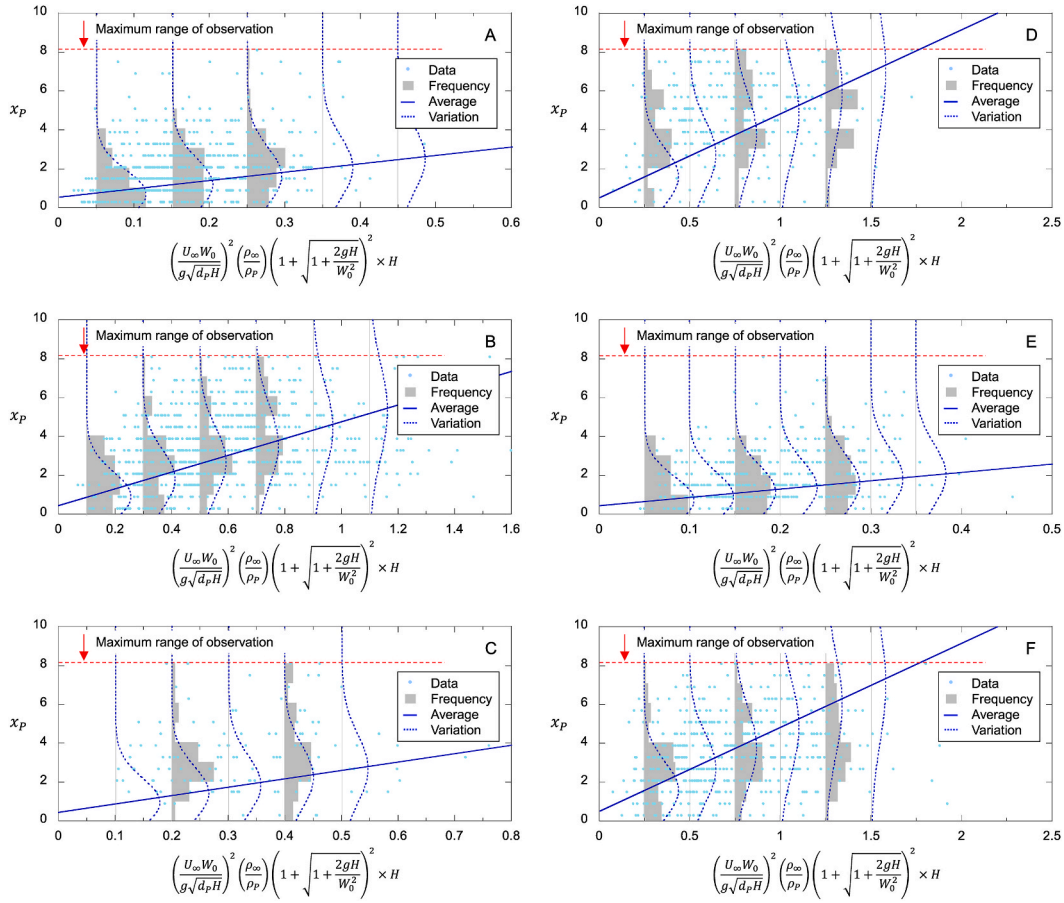
Fig. 15. Distribution of firebrand transport distance overlaid by result of estimated model.

$$\mu_i = aB_i^* H_i + b, \tag{18}$$

$$\sigma_i = cB_i^* H_i + d, \tag{19}$$

where x_{UB} is the upper bound of the observation (8.1 m in this experiment); a, b, c, and d are constants. For the calculation of B^*, the representative length of a firebrand, d_P, was obtained by taking the square root of $A_{P(Z)}$. In addition, although d_P should be calculated in units of (m) according to the rule of the SI unit system, d_P was calculated in the units of (cm) in this study considering the substantially small dimensions of the firebrands.

Table 6 displays the results of the parameter estimation. The value of $\widehat{R}$ for all the parameters was less than 1.1, which suggests that the MCMC simulation converged. As in the case with the projected area, $A_{P(Z)}$, the χ^2-test of goodness-of-fit at a significance level of 5% was performed to evaluate the agreement between the theoretical model and the measurement data. For all the cases, the results demonstrated that

Table 6
Result of parameter estimation for transport distance. Estimates are maximum a posteriori (MAP) estimates of posterior distributions. S.D. is the standard deviation; 2.5 % and 97.5 % are top and bottom bounds of the credible interval, respectively.

Parameter	Estimate	S.D.	2.5 %.	97.5 %.	$\widehat{R}$
a	4.34	0.23	3.90	4.80	1.00
b	0.48	0.16	0.15	0.78	1.00
c	1.21	0.69	0.06	2.36	1.00
d	1.15	0.15	0.07	2.24	1.00

the theoretical models were not statistically insignificant. The obtained model was added to Fig. 15, where the solid and dotted blue lines correspond to the mean and probabilistic variation, respectively. Although certain cases exhibited deviations, the estimated mean and probabilistic variation reproduced the measurement result reasonably in general.

5. Conclusions

In this study, the generation and transport processes of firebrands with a focus on their probabilistic variability were analyzed using a combustion apparatus installed in a boundary layer wind tunnel. The experimental parameters were the ejection height of firebrands, H, (1.08 and 1.48 m), crosswind velocity, U_∞, (1.5 and 3.0 m/s), and thickness of wood stick used for assembling wood cribs, d, (50 and 105 mm).

For the generation process, a deterministic relationship was derived for the projected area of the firebrand, $A_{P(Z)}$, based on simple physical considerations. The probabilistic variability of $A_{P(Z)}$ was evaluated by incorporating this relationship into the truncated exponential distribution. The firebrand density and weight proportion of the generated firebrands to the initial wood crib ranged from 29.7 to 74.5 kg/m^3 and 0.00526 %–0.0176 %, respectively.

For the transport process, a deterministic relationship was derived for the transport distance in the wind direction, x_P, based on simple physical considerations. The probabilistic variability of x_P was evaluated by incorporating this relationship into a truncated normal distribution.

In this experiment, the range of the data used for the model estimation was limited (e.g., the ejected velocity, W_0, ranged from 2.46 to 4.10 m/s; the cross-wind velocity, U_∞, ranged from 1.41 to 3.22 m/s; and the firebrands collected in the present experiment were generally

smaller than those collected in previous full-scale experiments). Hence, it would be beneficial to test the model under a broader range of conditions, especially under conditions similar to those of actual fires, to further improve the generality of the model. Furthermore, although the proposed models have been validated using experimental data for a structural fire scenario, the model is applicable for estimating the generation and transport behaviors of firebrands from other types of fire sources because the invoked assumptions are not scenario specific.

Author statement

Keisuke Himoto: Conceptualization, Methodology, Validation, Formal analysis, Investigation, Resources, Data curation, Writing, Visualization, Project administration, Funding acquisition, Tatsuya Iwami: Investigation, Resources.

Declaration of competing interest

The authors declare that they have no known competing financial interests or personal relationships that could have appeared to influence the work reported in this paper.

Acknowledgement

References

[1] E. Koo, P.J. Pagni, D.R. Weise, J.P. Woycheese, Firebrand and spotting ignition in large-scale fires, Int. J. Wildland Fire 19 (2010) 818–843, https://doi.org/10.1071/WF07119.

[2] A.C. Fernandez-Pello, Wildland fire spot by sparks and firebrands, Fire Saf. J. 91 (2017) 2–10, https://doi.org/10.1016/j.firesaf.2017.04.040.

[3] S.E. Caton, R.S.P. Hakes, M.J. Gollner, D.J. Gorham, A. Zhou, Review of pathway for building fire spread in the wildland urban interface, Fire Technol. 53 (2017) 429–473, https://doi.org/10.1007/s10694-016-0589-z.

[4] S.L. Manzello, S. Suzuki, M.J. Gollner, A.C. Fernandez-Pello, Role of firebrand combustion in large outdoor fire spread, Prog. Energy Combust. Sci. 76 (2020), https://doi.org/10.1016/j.pecs.2019.100801.

[5] Y. Ohmiya, T. Iwami, An investigation on the distribution of firebrands and spot fires due to a hotel fire, Fire Sci. Technol. 20 (2000) 27–35, https://doi.org/10.3210/fst.20.27.

[6] S.L. Manzello, E.I. Foote, Characterizing firebrand exposure from wildland-urban interface fires: results from the 2007 Angora fire, Fire Technol. 50 (2014) 105–124, https://doi.org/10.1007/s10694-012-0295-4.

[7] M. El Houssami, E. Mueller, J.C. Thomas, A. Simeoni, A. Filkov, N. Skowronski, M.R. Gallagher, K. Clark, R. Kremens, Experimental procedures characterizing firebrand generation in wildland fires, Fire Technol. 52 (2016) 731–751, https://doi.org/10.1007/s10694-015-0492-z.

[8] A. Filkov, S. Prohanov, E. Mueller, D. Kasymov, P. Martynov, M. El Houssami, J. Thomas, N. Skowronski, B. Butler, M. Gallagher, K. Clark, W. Mell, R. Kremens, R.M. Hadden, A. Simeoni, Investigation of firebrand production during prescribed fire conducted in a pine forest, Proc. Combust. Inst. 36 (2017) 3263–3270, https://doi.org/10.1016/j.proci.2016.06.125.

[9] S. Takeya, K. Himoto, T. Mizukami, K. Kagiya, T. Iwami, Report of the Survey on the Building Damage by the Large Fire Occurred in Itoigawa City, Niigata Prefecture on December 22, 2016, No. 980, Technical Note of National Institute for Land and Infrastructure Management, 2017. in Japanese).

[10] National Research Institute of Fire and Disaster, Survey report on the 2016 itoigawa fire, Report of NRIFD 84 (2018) (in Japanese).

[11] J.C. Thomas, E.V. Mueller, S. Santamaria, M. Gallagher, M. El Houssami, A. Filkov, K. Clark, N. Skowronski, R.M. Hadden, W. Mell, A. Simeoni, Investigation of firebrand generation from an experimental fire: development of a reliable data collection methodology, Fire Saf. J. 91 (2017) 864–871, https://doi.org/10.1016/j.firesaf.2017.04.002.

[12] S. Suzuki, S.L. Manzello, Characteristics of firebrands collected from actual urban fires, Fire Technol. 54 (2018) 1533–1546, https://doi.org/10.1007/s10694-018-0751-x.

[13] T.E. Waterman, Experimental study of firebrand generation, Final Technical Report, Project J 6130, OCD Work Unit 2536E (1969).

[14] H. Yoshioka, Y. Hayashi, H. Masuda, T. Noguchi, Real-scale fire wind tunnel experiment on generation of firebrands from a house on fire, Fire Sci. Technol. 23 (2004) 142–150, https://doi.org/10.3210/fst.23.142.

[15] S.L. Manzello, A. Maranghides, J.R. Shields, W. Mell, Y. Hayashi, D. Nii, Mass and size distribution of firebrands generated from burning Korean Pine (Pinus Koraiensis) trees, Fire Mater. 33 (2008) 21–31, https://doi.org/10.1002/fam.977.

[16] S. Miura, Y. Hayashi, Y. Ohmiya, T. Iwami, Experiments on firebrand generation, Proc, Annual Meeting of Architectural Institute of Japan (2011) 245–246 (in Japanese).

[17] S. Suzuki, S.L. Manzello, M. Lage, G. Laing, Firebrand generation data obtained from a full-scale structure burn, Int. J. Wildland Fire 21 (2012) 961–968, https://doi.org/10.1071/WF11133.

[18] B.W. Barr, O.A. Ezekoye, Thermo-mechanical modeling of firebrand breakage on a fractal tree, Proc. Combust. Inst. 34 (2013) 2649–2656, https://doi.org/10.1016/j.proci.2012.07.066.

[19] S. Suzuki, S.L. Manzello, Y. Hayashi, The size and mass distribution of firebrands collected from ignited building components exposed to wind, Proc. Combust. Inst. 34 (2013) 2479–2485, https://doi.org/10.1016/j.proci.2012.06.061.

[20] S. Suzuki, A. Brown, S.L. Manzello, J. Suzuki, Y. Hayashi, Firebrands generated from a full-scale structure burning under well-controlled laboratory conditions, Fire Saf. J. 63 (2014) 43–51, https://doi.org/10.1016/j.firesaf.2013.11.008.

[21] Y. Hayashi, T. Hebiishi, J. Izumi, T. Naruse, N. Itagaki, T. Hashimoto, N. Yasui, Y. Hasemi, Firebrand deposition and measurements of collected firebrands generated and transported from a full-scale burn test using a large wooden building, AIJ Journal of Technology and Design 20 (2014) 605–610, https://doi.org/10.3130/aijt.20.605, in Japanese.

[22] A. Tohidi, N. Kaye, W. Bridges, Statistical description of firebrand size and shape distribution from coniferous trees for use in Metropolis Monte Carlo simulations of firebrand flight distance, Fire Saf. J. 77 (2015) 21–35, https://doi.org/10.1016/j.firesaf.2015.07.008.

[23] S.L. Manzello, S. Suzuki, Generating wind-driven firebrand showers characteristic of burning structures, Proc. Combust. Inst. 36 (2017) 3247–3252, https://doi.org/10.1016/j.proci.2016.07.009.

[24] S.E. Caton-Kerr, A. Tohidi, M.J. Gollner, Firebrand generation from thermally-degraded cylindrical wooden dowels, Front. Mech. Eng. 5 (2019), https://doi.org/10.3389/fmech.2019.00032.

[25] F. Hedayati, B. Bahrani, A. Zhou, S.L. Quarles, D.J. Gorham, A framework to facilitate firebrand characterization, Front. Mech. Eng. 5 (2019), https://doi.org/10.3389/fmech.2019.00043.

[26] C.S. Tarifa, P.P. del Notario, F.G. Moreno, On the flight paths and lifetimes of burning particles of wood, Symposium (International) on Combustion 10 (1965) 1021–1037, https://doi.org/10.1016/S0082-0784(65)80244-2.

[27] C.S. Tarifa, Transport and Combustion of Firebrands, Final Report of Grants FG-SP-114 and GD-SP-146, 1967.

[28] S.L. Lee, J.M. Hellman, Study of firebrand trajectories in a turbulent swirling natural convection plume, Combust. Flame 13 (1969) 645–655, https://doi.org/10.1016/0010-2180(69)90072-8.

[29] S.L. Lee, J.M. Hellman, Firebrand trajectory study using an empirical velocity-dependent burning law, Combust. Flame 15 (1970) 265–274, https://doi.org/10.1016/0010-2180(70)90006-4.

[30] A. Muraszew, J.B. Fedele, Statistical model for sport fire hazard, Aerospace Report, ATR-77(7588)-1 (1976).

[31] A. Muraszew, J.B. Fedele, Trajectory of firebrands in and out of fire whirls, Combust. Flame 30 (1977) 321–324, https://doi.org/10.1016/0010-2180(77)90081-5.

[32] F.A. Albini, Spot Fire Distance from Burning Trees, USDA Forest Service, 1979. General Technical Report INT-56.

[33] F.A. Albini, Transport of firebrands by line thermals, Combust. Sci. Technol. 32 (1983) 277–288, https://doi.org/10.1080/00102208308923662.

[34] J.P. Woycheese, P.J. Pagni, D. Liepmann, Brand propagation from large-scale fires, J. Fire Protect. Eng. 10 (1999) 32–44, https://doi.org/10.1177/104239159901000203.

[35] R.A. Anthenien, S.D. Tse, A.C. Fernandez-Pello, On the trajectories of embers initially elevated or lofted by small scale ground fire plumes in high winds, Fire Saf. J. 41 (2006) 349–363, https://doi.org/10.1016/j.firesaf.2006.01.005.

[36] H.H. Wang, Analysis on downwind distribution of firebrands sourced from a wildland fire, Fire Technol. 47 (2011) 321–340, https://doi.org/10.1007/s10694-009-0134-4.

[37] K. Himoto, T. Tanaka, Transport of disk-shaped firebrands in a turbulent boundary layer, Fire Saf. Sci. 8 (2005) 433–444, https://doi.org/10.3801/IAFSS.FSS.8-433.

[38] H. Huang, R. Ooka, S. Kato, Y. Hayashi, A numerical study of firebrands scattering in urban fire based on CFD and firebrands aerodynamics measurements, J. Fire Sci. 25 (2007) 355–378, https://doi.org/10.1177/0734904107073008.

[39] N. Sardoy, J.L. Consalvi, B. Porterie, A.C. Fernandez-Pello, Modeling transport and combustion of firebrands from burning trees, Combust. Flame 150 (2007) 151–169, https://doi.org/10.1016/j.combustflame.2007.04.008.

[40] N. Sardoy, J.L. Consalvi, A. Kaiss, Porterie B. Fernandez-Pello, Numerical study of ground-level distribution of firebrands generated by line fires, Combust. Flame 154 (2008) 478–488, https://doi.org/10.1016/j.combustflame.2008.05.006.

[41] S. Kortas, P. Mindykowski, J.L. Consalvi, H. Mhiri, B. Porterie, Experimental validation of a numerical model for the transport of firebrands, Fire Saf. J. 44 (2009) 1095–1102, https://doi.org/10.1016/j.firesaf.2009.08.001.

[42] E. Koo, R.R. Linn, P.J. Pagni, C.B. Edminster, Modelling firebrand transport in wildfires using HIGRAD/FIRETEC, Int. J. Wildland Fire 21 (2012) 396–417, https://doi.org/10.1071/WF09146.

[43] A. Tohidi, N. Kaye, Stochastic modeling of firebrand shower scenarios, Fire Saf. J. 91 (2017) 91–102, https://doi.org/10.1016/j.firesaf.2017.04.039.

[44] R. Wadhwani, D. Sutherland, A. Ooi, K. Moinuddin, G. Thorpe, Verification of a Lagrangian particle model for short-range firebrand transport, Fire Saf. J. 91 (2017) 776–783, https://doi.org/10.1016/j.firesaf.2017.03.019.

[45] P.F. Ellis, The Aerodynamic and Combustion Characteristics of Eucalypt Bark – a Firebrand Study, Ph.D Thesis, Australian National University, 2000.

[46] S.L. Manzello, J.R. Shields, T.G. Clearly, A. Maranghides, W.E. Mell, J.C. Yang, Y. Hayashi, D. Nii, T. Kurita, On the development and characterization of a firebrand generator, Fire Saf. J. 43 (2008) 258–268, https://doi.org/10.1016/j.firesaf.2007.10.001.

[47] A. Tohidi, N.B. Kaye, Comprehensive wind tunnel experiments of lofting and downwind transport of non-combusting rod-like model firebrands during firebrand shower scenarios, Fire Saf. J. 90 (2017) 95–111, https://doi.org/10.1016/j.firesaf.2017.04.032.

[48] J. Song, N. Liu, H. Li, L. Zhang, X. Huang, The wind effect on the transport and burning of firebrands, Fire Technol. 53 (2017) 1555–1568, https://doi.org/10.1007/s10694-017-0647-1.

[49] M.A. Finney, FARSITE: Fire Area Simulator – Model Development and Evaluation, RMRS-RP-4, USDA, 1998.

[50] R. Linn, J. Reisner, J.J. Coleman, J. Winterkamp, Studying wildfire behavior using FIRETEC, Int. J. Wildland Fire 11 (2002) 233–246, https://doi.org/10.1071/WF02007.

[51] W. Mell, M.A. Jenkins, J. Could, P. Cheney, A physics-based approach to modelling grassland fires, Int. J. Wildland Fire 16 (2007) 1–22, https://doi.org/10.1071/WF06002.

[52] K. Himoto, T. Tanaka, Development and validation of a physics-based urban fire spread model, Fire Saf. J. 43 (2008) 477–494, https://doi.org/10.1016/j.firesaf.2007.12.008.

[53] S.W. Lee, R.A. Davidson, Physics-based simulation model of post-earthquake fire spread, J. Earthq. Eng. 14 (2010) 670–687, https://doi.org/10.1080/13632460903336928.

[54] S. Zhao, Simulation of mass fire-spread in urban densely built areas based on irregular coarse cellular automata, Fire Technol. 47 (2011) 721–749, https://doi.org/10.1007/s10694-010-0187-4.

[55] K. Himoto, K. Mukaibo, R. Kuroda, Y. Akimoto, A. Hokugo, T. Tanaka, A post-earthquake fire spread model considering damage of building components due to seismic motion and heating of fire, Fire Saf. Sci. 10 (2011) 1319–1330, https://doi.org/10.3801/IAFSS.FSS.10-1319.

[56] G. Thomas, D. Heron, J. Cousins, M. de Roiste, Modeling and estimating post-earthquake fire spread, Earthq. Spectra 28 (2012) 795–810, https://doi.org/10.1193/1.4000009.

[57] H. Yoshioka, K. Himoto, K. Kagiya, Large urban fires in Japan: history and management, Fire Technol. 56 (2020) 1885–1901, https://doi.org/10.1007/s10694-020-00960-8.

[58] K. Himoto, K. Harada, Foreseeability of collapse of wooden buildings based on the behavior of fire observed from outdoors, The AIJ Journal of Technology and Design 17 (2011) 191–194, https://doi.org/10.3130/aijt.17.191, in Japanese.

[59] K. Himoto, Quantification of cross-wind effect on temperature elevation in the downwind region of fire sources, Fire Saf. J. 106 (2019) 114–123, https://doi.org/10.1016/j.firesaf.2019.04.010.

[60] G. Heskestad, Modeling of enclosure fires, Proc. Symposium (International) on Combustion 14 (1973) 1021–1030.

[61] C. Hugget, Estimation of rate of heat release by means of oxygen consumption method, Fire Mater. 4 (1980) 61–65, https://doi.org/10.1002/fam.810040202.

[62] A. Gelman, J.B. Carlin, H.S. Stern, D.B. Dunson, A. Vehtari, D.B. Rubin, Bayesian Data Analysis, third ed., CRC Press, 2013.